Chinese Chemical Letters 34 (2023) 108273

Contents lists available at ScienceDirect

Chinese Chemical Letters

journal homepage: www.elsevier.com/locate/cclet

An ESIPT-based NIR-fluorescent probe for exosome labeling and *in situ* imaging

Jipeng Ding[a,1], Runsha Xiao[b,c,1], Anyao Bi[a], Guanyang Chen[d], Nengwei Zhang[d], Zihua Chen[b,c], Xueping Feng[b,c,*], Wenbin Zeng[a,*]

[a] Xiangya School of Pharmaceutical Sciences, Central South University, Changsha 410013, China
[b] Department of Gastrointestinal Surgery, Hunan Key Laboratory of Precision Diagnosis and Treatment of Gastrointestinal Tumor, Xiangya Hospital, Central South University, Changsha 410013, China
[c] Institute of Medical Sciences, Xiangya Hospital, Central South University, Changsha 410013, China
[d] Peking University Ninth School of Clinical Medicine (Beijing Shijitan Hospital, Capital Medical University), Beijing 100038, China

ARTICLE INFO

Article history:
Received 18 November 2022
Revised 19 February 2023
Accepted 27 February 2023
Available online 2 March 2023

Keywords:
Exosome
Fluorescent probe
Excited state intramolecular proton transfer
Gastric cancer
Bioimaging

ABSTRACT

Exosomes play significant roles in physiological and tumorigenic processes and it is desirable to visualize and track the exosomes. Herein, a novel amphiphilic fluorescent probe **HBT-Exo** based on excited-state intramolecular proton transfer (ESIPT) mechanism is reported for exosome-labeling. Its ESIPT characteristics were confirmed by both theory calculation and experimental observation, which enable the probe to show a large Stokes shift as well as near-infrared (NIR) keto-form emission. **HBT-Exo** displayed excellent biocompatibility and remarkable efficiency for exosome-labeling in gastric cancer cells. Furthermore, the labeled exosomes were successfully applied for the real-time *in situ* imaging in mouse models.

Exosomes are 30–150 nm-sized, cell-derived extracellular vesicles (EVs) with a lipid bilayer membrane that originated from multivesicular bodies (MVBs) in most somatic cells [1]. They contain various origin cell-specific intracellular molecules such as mRNA, miRNA as well as proteins. Accumulating studies revealed that exosomes play a significant role in intercellular communication [2]. These studies reveal that exosomes can modulate not only the surrounding environment but also the characteristics of the cells around or at a distance [3,4]. Thereby, the investigation of exosomes has the potential to identify unknown cellular and molecular mechanisms of intercellular communication, organ homeostasis and tumorigenesis [5–8]. Since exosomes are homologous to their parent cells, they share some traits with their cells of origin [9]. In addition, exosomes derived by tumor cells show unique tumor targeting abilities due to homing effect and the presentation of tumor-specific antigens [10–12]. This indicated that it is feasible to apply exosomes as a specific targeting tool for drug delivery, especially for cancer therapeutics. Importantly, recently exosomes are reported as a potential candidate for the next generation's drug delivery carrier due to its low immunogenicity, low toxicity, high biocompatibility, and high stability in biological systems [13,14]. Nevertheless, to disclose the role of exosomes, it is of significance to visualize the exosomes and trace the distribution and movement of it both *in vitro* and *in vivo* [15–17]. Thus, it is highly desirable to develop novel materials to efficiently label exosomes for real-time imaging.

Fluorescence imaging is a promising tool for visualizing the physiological and pathological processes in biological systems with high efficiency [18]. Small organic molecular fluorophores with high sensitivity and quantum efficiency provide a chemical tool for biological imaging [19]. For exosome-labeling, common commercial fluorescent dyes, such as Paul Karl Horan (PKH) family (PKH26 and PKH67) and Di family (DiO and DiI), with hydrophobic properties can bind to the outer lipid bilayer of the exosomes to present strong fluorescence. However, those dyes exhibit a short Stokes shift and their fluorescent intensity can be interfered due to continuous self-absorption [20,21]. Some dyes like CFDA-SE shows good water solubility. However, without the introduction of sulfonate group, the classic cyanine-based dyes with low water solubility can easily form self-assembly nanoparticles in an aqueous environment thus generating false-positive fluorescent signal. Since the differentiation of self-assembly nanoparticles is arduous, additional removal steps are suggested to eliminate the interference of the aggerated dyes [22,23]. Besides, most of dyes with short emissions are limited for further biological applications, such as *in vivo*

* Corresponding authors.
E-mail addresses: fxp1029@aliyun.com (X. Feng), wbzeng@hotmail.com (W. Zeng).
[1] These authors contributed equally to this work.

https://doi.org/10.1016/j.cclet.2023.108273
1001-8417/

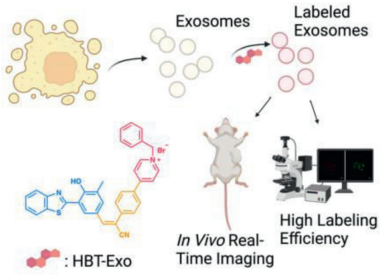

Scheme 1. Schematic illustration of **HBT-Exo** as a fluorescence exosome-labeling tool.

animal imaging. Therefore, it is still challenging to develop novel exosome-labeling probes with excellent photophysical properties.

Fluorescent fluorophores with excited-state intramolecular proton transfer (ESIPT) properties undergo a unique four-stage fast phototautomerization process (Enol→Enol*→Keto*→Keto) upon photo-excitation. Upon this photochemical process, ESIPT fluorophores present a large Stokes shift and avoid self-reabsorption and inner-filter effects, which are suitable for fluorescent imaging and sensing. 2-(2-Hydroxyphenyl)benzoxazole (HBO) and 2-(2-hydroxyphenyl)benzothiazole (HBT) are typical ESIPT fluorophores [24]. Fluorophores with near-infrared (NIR) emission show deeper penetration depth and lower tissue lesions than those with visible wavelengths. For the construction of fluorescent molecules with NIR emission, intramolecular charge transfer (ICT) is an effective approach that can be achieved by the introduction of "D-π-A" structure [25]. In this work, we combined the philosophies of ESIPT and ICT to construct a novel amphiphilic probe, (*E*)-4-(4-(2-(3-(benzo[*d*]thiazol-2-yl)-4–hydroxy-5-methylphenyl)-1-cyanovinyl) phenyl)-1-benzylpyridin-1-ium bromide (**HBT-Exo**), which can anchor on the exosomes' negatively charged lipid membranes to achieve efficient exosome-labeling. The design of the structure of the probe was guided by "D-π-A" strategy. HBT served as ESIPT functional group as well as electron-donating unit. The elongation of the conjugation was achieved by the introduction of carbon-carbon double bond and benzene. Pyridinium group serves as the electron-withdrawing unit and hydrophilic unit. As depicted in Scheme 1, **HBT-Exo** could serve as a fluorescence exosome-labeling tool. Compared with traditional exosomes probes with low water solubility, **HBT-Exo** presents the amphiphilic property. Furthermore, it is discovered that **HBT-Exo** displayed low cytotoxicity and remarkable exosome-labeling efficiency.

The preparation of **HBT-Exo** is achieved *via* 5 step reactions, as shown schematically in Scheme S1 (Supporting information). The formylation of HBT afforded compound **2**, and it was followed by a Knoevenagel condensation reaction and a Suzuki coupling reaction to give compound **4**. The final probe was yielded by an ionization reaction of compound **4**. The physiochemical structure of **HBT-Exo** was confirmed by NMR and high-resolution mass spectrometry.

The optical property of **HBT-Exo** was then carried out. The probe shows a typical dual-emission in different organic solvents due to the distinctive ESIPT process. The enol-form emission was found at 450 nm. As known, the keto-form emission was crucial broad, with an observed ranged from 400 nm to 800 nm. However, in a DMSO solvent, keto emission was the dominant peak with a jumped peak at 665 nm (Fig. 1a). Nevertheless, **HBT-Exo** exhibits a large Stokes shift (>200 nm) by taking advantage of the ESIPT process. The shifts of fluorescent emission in various solvents indicate the typical ICT property (Fig. S1 in Supporting information). Next, the photostability of **HBT-Exo** was investigated. As for long-time fluorescent labeling, the anti-photobleaching ability of the dye is of great significance. The photostability assay was conducted under continuous excitation at 370 nm by using Xe lamp (10 mW/cm^2) for 30 min. As shown in Fig. 1b, during the irradiation, the fluorescence intensity witnessed a negligible attenuation. As depicted in Fig. S2 (Supporting information), after a total irradiation time of 30 min, the fluorescence intensity slightly dropped to 93.8% of its initial signal intensity. Fig. S3 (Supporting information) presented the effect of pH on the fluorescence intensity of **HBT-Exo**, which indicated that the probe could work both in normal physiological environment and weakly acidic environment.

The ICT and ESIPT mechanisms are further verified through theory calculation by using DFT and (TD) DFT at the level of

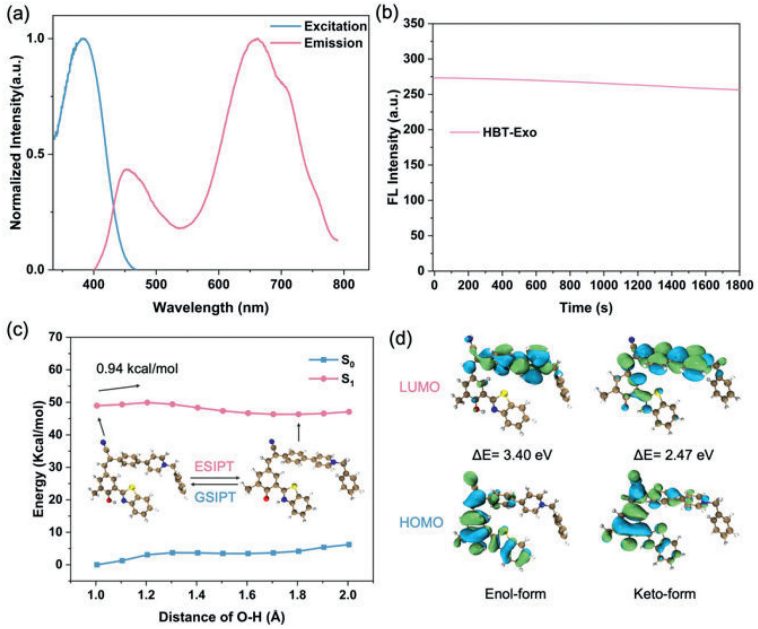

Fig. 1. (a) Normalized excitation and emission wavelength of **HBT-Exo** (10 μmol/L) in DMSO. (b) The fluorescence intensities of **HBT-Exo** exposed to 370 nm irradiation at different time. (c) Potential energy surfaces (PESs) of the S_0 and S_1 states as functions of the strength of O–H bond. (d) Frontier molecular orbitals of the enol-form and keto-form. ΔE (energy gap) = $E_{LUMO} - E_{HOMO}$.

PBE0/Def2-svp. The potential energy surfaces (PESs) can reveal the ESIPT and GSIPT process of **HBT-Exo** [26,27]. As shown in Fig. 1c, PESs of the S_0 and S_1 states as functions of the strength of O–H bond. The keto-form exhibits a lower S_1 energy and a higher S_0 energy. The energy barrier in the S_1 profile was relatively low (0.94 kcal/mol). Thus, the transfer of enol-form to keto-form in the S_1 state occurs easily. The keto-form in the S_1 state then relaxed to S_0 state, followed by a nearly barrierless pathway that backward to the enol-form. This strongly demonstrates the ESIPT process of **HBT-Exo**, which is in accordance with the experimental observation. The frontier molecular orbitals in Fig. 1d show the distinct charge separation on the molecule which indicates the ICT property [28]. As for the highest occupied molecular orbital (HOMO) of **HBT-Exo**, the charges are mostly populated in the HBT region, whereas the charges markedly shift to the cyanostyryl part in lowest unoccupied molecular orbital (LUMO). The energy gap between HOMO and LUMO of the keto-form is 2.47 eV, which is significantly lower than the one of the enol-form (3.40 eV). This energy gap difference accounts for the redshift of the fluorescent emission of the keto-form.

To meet the demands of further biological studies, the biosafety of **HBT-Exo** was investigated. MTT assay with 3-(4,5-dimethylthiazol-2-yl)-2,5-diphenyl tetrazolium bromide was conducted to evaluate the cytotoxicity of **HBT-Exo**. As shown in Fig. S4 (Supporting information), there is no significant cytotoxicity when the concentration of **HBT-Exo** ranged from 1 μmol/L to 50 μmol/L after incubation with AGS cells for 48 h. The cell viability decreased only when the concentration of the probe was extremely high (100 μmol/L). The MTT assay indicates the good biosafety of the **HBT-Exo**.

The physicochemical and biochemical properties of both labeled and non-labeled exosomes were analyzed by using Western blot (WB), transmission electron microscopy (TEM), nanoparticle tracking analysis (NTA) and flow cytometry (FC). WB results showed that both labeled and non-labeled exosomes expressed the positive exosomes markers heat shock protein 70 (HSP70) and endosomal membrane proteins TSG101 (Fig. 2a) [29]. Besides, the negative marker Calnexin was not expressed in both samples, which demonstrates the pure purification of the exosomes [30]. For the morphology study, as shown in Figs. 2b and c, the TEM results indicates that exosomes were spherical in shape and the labeling by **HBT-Exo** does not change the morphology of the exosomes. Furthermore, NTA revealed that the size of the labeled exosomes is comparable to unlabeled exosomes (Fig. S5 in Supporting information). These results demonstrate that the labeling by **HBT-Exo** do not change the general physicochemical and biochemical properties of exosomes. To further evaluate the labeling efficacy, PBS suspensions of exosomes derived from AGS cells were carried out for FC. As shown in Fig. 3d, exosomes treated or untreated by **HBT-Exo** were analyzed. Analyses were carried out by choosing 405 nm as the excitation wavelength and red channel for recording. The recorded fluorescence intensity of the control group (NC, without labeling) was at a low background level of autofluorescence. In contrast, the emission intensity of the labeled exosomes (P for 72 h, M for 1 h) was significantly higher. Both 1 h and 72 h groups showed high fluorescent intensity which demonstrated the efficient labeling ability of **HBT-Exo**.

The labeling efficacy of **HBT-Exo** was further confirmed by confocal laser scanning microscopy (CLSM). First, the membrane affinity capacity of the probe was studied. Fig. S6 (Supporting

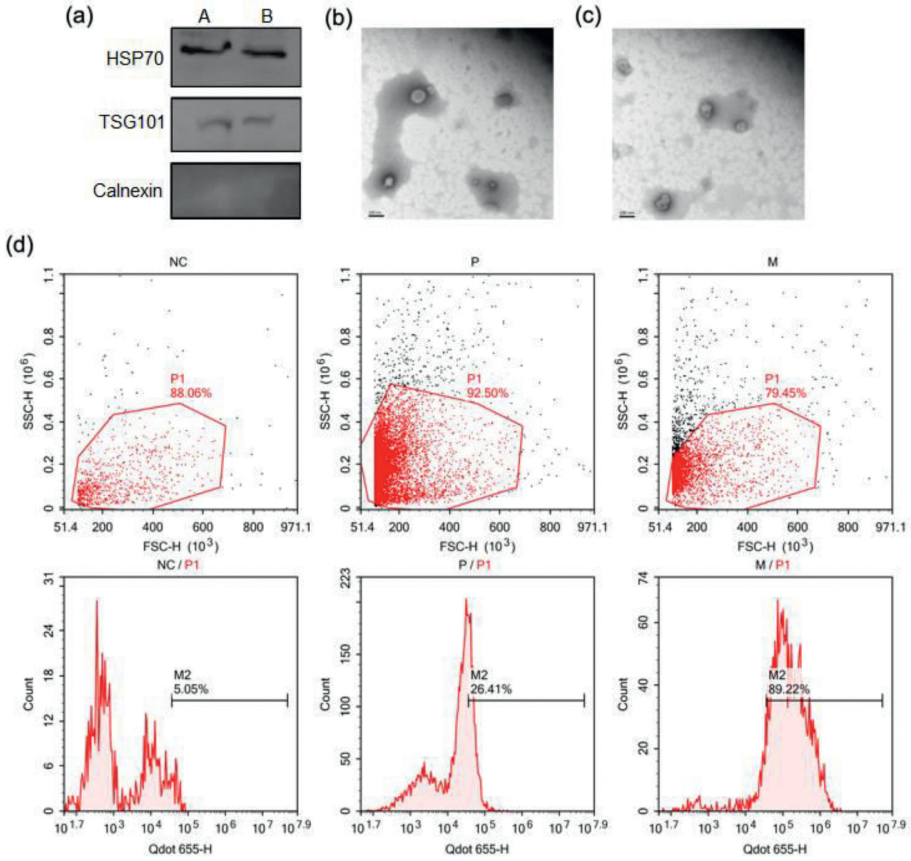

Fig. 2. (a) Major protein markers of exosomes labeled by **HBT-Exo** (A) or without labeling (B) detected by Western blot. (b, c) TEM images of non-labeled exosomes and labeled exosomes, respectively. Scale bar: 100 nm. (d) Exosomes labeled with **HBT-Exo** analyzed by flow cytometry.

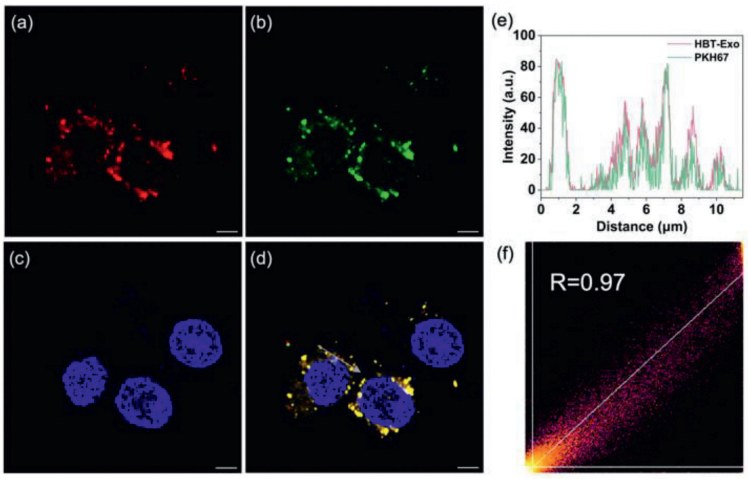

Fig. 3. CLSM image of the exosomes stained by (a) **HBT-Exo**, (b) PKH67 and (c) DAPI. (d) Merged image of (a–c). Scale bar: 5 μm. (e) Quantification analysis of the fluorescence intensity distribution of the arrow in (d). (f) The Pearson correlation coefficient for the fluorescent signal of **HBT-Exo** and PKH67. Blue channel: λem = 450 ± 20 nm, λex = 365 nm. Green channel: λem = 500 ± 20 nm, λex = 490 nm. Red channel: λem = 650 ± 20 nm, λex = 405 nm.

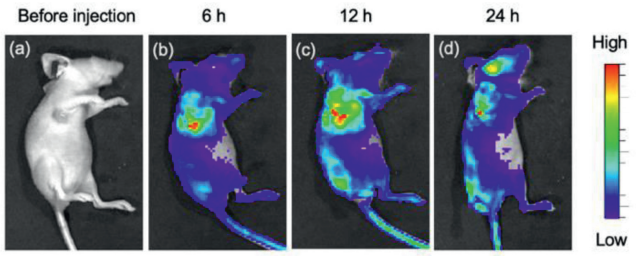

Fig. 4. Representative time-dependent *in vivo* fluorescence images of tumor-bearing mice through the administration of **HBT-Exo** labeled exosomes: (a) before injection, (b) 6 h, (c) 12 h and (d) 24 h.

information) showed that AGS, which is a kind of GC cell, can absorb the **HBT-Exo** and stain the cell membrane. In addition, the popular commercial dye PKH67 was applied to co-stained with **HBT-Exo**. Exosomes were incubated with **HBT-Exo**, PKH67 and 4′,6-diamidino-2-phenylindole (DAPI). **HBT-Exo** and PKH67 were added and incubated in the cell dishes for 24 h. The green fluorescence signal emitted by PKH67 overlapped with **HBT-Exo**'s red signal (Figs. 3a–d). As shown in Fig. 3e, quantification analysis of the line fluorescence intensity distribution indicates the distinguished colocalization between the red channel and the green channel. In addition, the Pearson correlation coefficient for **HBT-Exo** and PKH67 is 0.97 (Fig. 3f), which demonstrates the excellent colocalization of the fluorescence of **HBT-Exo** with that of PKH67.

To investigate whether **HBT-Exo** could be used to label exosomes *in vivo*, animal experiments were then conducted. All animal experiments were performed according to the relevant ethical regulations of Central South University, and this study received approval from Central South University Experimental Animal Ethics Committee. Due to the homogenous property of tumor cells and their exocytosed exosomes, the tumor-derived exosomes can target corresponded tumor tissue through homing effect [31–33]. In this case, the tumor-bearing mice were successfully established by injecting a total of 5×10^6 AGS cells into the underarm of the BALB/c nude mouse. The **HBT-Exo** labeled AGS cell derived exosomes were injected into the tumor-bearing mice through the tail vein at different intervals before *in vivo* fluorescence imaging. As shown in Figs. 4a–d, after 6 h post-injection, the labeled exosomes displayed a certain intensity signal at the tumor site. In addition, the fluorescence signal intensity of the 12 h post-injection group was higher than that of the 6 h group. Importantly, for 24 h post-injection, the fluorescence signal intensity at the tumor site still could be observed. *Ex-vivo* imaging of major organs dissected after 12 h post-injection shows that the liver exhibits the highest signal, followed by the kidneys, spleen, and tumor (Fig. S7 in Supporting information). These data together proved that **HBT-Exo** could be used as a stable chemical dye for long-time *in vivo* imaging.

In conclusion, we successfully designed a novel amphiphilic fluorescent probe, **HBT-Exo**, which is capable of specific exosome-labeling and tracing. Its ESIPT characteristics were confirmed by both theory calculation and experimental observation, which enable the probe to show a large Stokes shift as well as NIR ketoform emission. Besides, **HBT-Exo** performed low cytotoxicity, high photostability and could easily label the exosomes derived from GC cells in a mild PBS solution. By taking advantage of the homing effect of exosomes, *in situ* real-time tumor imaging is achieved through the administration of fluorescent labeled exosomes. Considering its label efficiency and versatility *in vitro* and *in vivo*, **HBT-Exo** could serve as an alternative tool that provide a new avenue for further biomedical research and clinical application.

Declaration of competing interest

The authors declare that they have no known competing financial interests or personal relationships that could have appeared to influence the work reported in this paper.

Acknowledgments

The authors gratefully acknowledge the financial support from the National Natural Science Foundation of China (Nos. 82272067, 81974386 and M-0696), Research and Development program in Key Areas of Hunan Province (No. 2019SK2143), Natural Science Foundation of Hunan Province (Nos. 2022JJ80052 and 2022JJ30920).

Supplementary materials

Supplementary material associated with this article can be found, in the online version, at doi:10.1016/j.cclet.2023.108273.

References

[1] K. Jiang, Y. Wu, J. Chen, et al., Chin. Chem. Lett. 32 (2021) 1827–1830.
[2] D.M. Pegtel, S.J. Gould, Annu. Rev. Biochem. 88 (2019) 487–514.

[3] J. Dai, Y. Su, S. Zhong, et al., Signal. Transduct. Target. Ther. 5 (2020) 145.
[4] Z. Fang, X. Zhang, H. Huang, et al., Chin. Chem. Lett. 33 (2022) 1693–1704.
[5] P.D. Stahl, G. Raposo, Physiology 34 (2019) 169–177.
[6] I. Shoucair, F.M. Weber, J. Jabalee, S. Maleki, C. Garnis, Int. J. Mol. Sci. 21 (2020) 6837–6874.
[7] N. Milman, L. Ginini, Z. Gil, Drug Resist. Updat. 45 (2019) 1–12.
[8] X. Wang, Z. Xiang, G.S.W. Tsao, W. Tu, Cell. Mol. Immunol. 18 (2021) 501–503.
[9] A.A. Farooqi, N.N. Desai, M.Z. Qureshi, et al., Biotechnol. Adv. 36 (2018) 328–334.
[10] L. Qiao, S. Hu, K. Huang, et al., Theranostics 10 (2020) 3474–3487.
[11] A. Thakur, D.C. Parra, P. Motallebnejad, M. Brocchi, H.J. Chen, Bioact. Mater. 10 (2022) 281–294.
[12] I.K. Herrmann, M.J.A. Wood, G. Fuhrmann, Nat. Nanotechnol. 16 (2021) 748–759.
[13] E.J. Bunggulawa, W. Wang, T. Yin, et al., J. Nanobiotechnol. 16 (2018) 81.
[14] P. Fu, J. Zhang, H. Li, et al., Adv. Drug Deliv. Rev. 179 (2021) 113910.
[15] H. Cao, Z. Yue, H. Gao, et al., ACS Nano 13 (2019) 3522–3533.
[16] J. Chen, M. Xie, M. Shi, et al., Anal. Chem. 94 (2022) 2227–2235.
[17] J. Chen, J. Tang, H. Meng, et al., Chem. Commun. 56 (2020) 9024–9027.
[18] H. Li, H. Kim, F. Xu, et al., Chem. Soc. Rev. 51 (2022) 1795–1835.
[19] H.H. Han, H. Tian, Y. Zang, et al., Chem. Soc. Rev. 50 (2021) 9391–9429.
[20] Y.W. Yi, J.H. Lee, S.Y. Kim, et al., Int. J. Mol. Sci. 21 (2020) 665–688.
[21] C. Han, J. Zhou, C. Liang, et al., Biomater. Sci. 7 (2019) 2920–2933.
[22] P.P. Dominkuš, M. Stenovec, S. Sitar, et al., Biochim. Biophys. Acta Biomembr. 1860 (2018) 1350–1361.
[23] J. Wang, D. Chen, E.A. Ho, J. Control. Release 329 (2021) 894–906.
[24] A.C. Sedgwick, L. Wu, H.H. Han, et al., Chem. Soc. Rev. 47 (2018) 8842–8880.
[25] X. Luo, J. Li, J. Zhao, et al., Chin. Chem. Lett. 30 (2019) 839–846.
[26] B. Feng, Y. Zhu, J. Wu, et al., Chin. Chem. Lett. 32 (2021) 3057–3060.
[27] T. Lu, F. Chen, J. Comput. Chem. 33 (2012) 580–592.
[28] M. Liu, R. Xiao, B. Feng, et al., Sens. Actuators B: Chem. 342 (2021) 130038.
[29] R. Kalluri, J. Clin. Investig. 126 (2016) 1208–1215.
[30] H. Miyake, C. Lee, S. Chusilp, et al., Surg. Int. 36 (2020) 155–163.
[31] J. Han, L. Zhang, M. Cui, et al., Anal. Chem. 93 (2021) 10122–10131.
[32] Y. Duo, D. Zhu, X. Sun, et al., Biomaterials 272 (2021) 120755.
[33] J. Liu, K. Yi, Q. Zhang, et al., Small 17 (2021) 2104585.